

Revani diffusion model in  $\text{Cu}(\text{In,Ga})\text{Se}_2$ Cite this: *J. Mater. Chem. A*, 2023, 11, 26426Diego Colombara,<sup>a</sup> Billy J. Stanbery<sup>b</sup> and Giovanna Sozzi<sup>c</sup>Received 23rd June 2023  
Accepted 24th November 2023

DOI: 10.1039/d3ta03690a

rsc.li/materials-a

The commercial attractiveness of  $\text{Cu}(\text{In,Ga})(\text{S,Se})_2$  (CIGS) photovoltaics is still curtailed by the R&D gap that separates it from silicon. Overcoming the gap requires the pursuit of strategic approaches, leaving plenty of room for R&D at both industrial and lab scale. Yet, its technological progress hinges on our understanding of the diffusion phenomena that occur during and after the absorber growth, particularly in combination with alkali metal doping. This contribution introduces a simplified model of atomic diffusion in CIGS based on insights drawn from recent and older (but crucial) literature. The concept of anisotropy-induced fluctuations emerges. We hypothesize that grain-dependent inhomogeneities arise in CIGS devices because of crystallographic dependent alkali metal diffusivities. Numerical simulations reveal that inhomogeneous doping density and CdS buffer layer thickness may impair the device performance by up to more than 1% absolute efficiency.

## 1. Introduction

At 23.6%, CIGS cells are the most efficient among the commercially available polycrystalline thin film technologies.<sup>1</sup> Very high efficiencies are attained with two distinct deposition strategies, both of which are employed industrially for module manufacturing: reactive annealing of metal precursors,<sup>2</sup> and elemental co-evaporation.<sup>3</sup> CIGS is also deposited on flexible substrates such as stainless steel foils and even polymers.<sup>4</sup> This is particularly attractive for building-integrated applications, which is expected to become compulsory for new constructions in Europe and certain US states.

One appealing prospect is to deploy CIGS as a low-bandgap partner to higher bandgap semiconductors such as metal halide perovskites,<sup>5</sup> with the aim of developing tandem cells with a Shockley–Queisser (SQ) efficiency limit of 46%.

However, the high record efficiencies at laboratory cell scale are still lagging 3.4 percent points behind the competitive silicon technology. This efficiency gap is also transferred at module level,<sup>6</sup> mainly due to resistive losses in the front transparent conductive oxide (TCO) that become important when passing from small to large areas. In tandem applications, utilizing low-bandgap CIGS with reduced short circuit photocurrent density mitigates significantly the impact of these TCO resistive losses.

A long-sought approach to solve this conundrum is to develop wider-gap CIGS, as this would increase the voltage and decrease the electrical current, hence the resistive losses in the TCO. Efficient wider-gap CIGS would also serve as a stable top

junction in tandem cells. This so-called *chalcopyrite* material allows bandgap widening by simply increasing the relative concentration of gallium compared to indium or sulfur compared to selenium. Nevertheless, achieving highly efficient wider-gap CIGS cells has been very challenging, due to significant voltage losses.<sup>7–9</sup> Recently, advances have been achieved on both S-rich<sup>10</sup> and Ga-rich<sup>11</sup> CIGS cells through processing changes to minimize the scale of spatially varying disorder – a major root cause of voltage deficit – and silver alloying as an effective strategy to improve crystal quality.

Conceivably, if recent advances in wider-gap CIGS devices, as well as trends and limitations of today's narrow-gap CIGS devices can be understood, and the path towards SQ parity can be identified, holistic insights into the material will be learned, for the benefit of the technology as a whole.<sup>12</sup> Herein, a *revani* † model of atomic diffusion is presented to account for both recent and older overlooked evidence and suggest the crucial link to CIGS device performance.

## 2. Do we really understand alkali metal doping?

The efficiency deficit of record CIGS from the viewpoint of carrier management (expressed as the product  $ff \times V_{\text{OC}}$ , fill factor times open circuit voltage<sup>13</sup>) is approximately 24% relative to SQ. This deficit is larger for CdTe (conservative estimate: 28% relative), but considerably lower for silicon (*ca.* 16% relative). Therefore, research is being devoted to understanding its origin, particularly relating to  $V_{\text{OC}}$ .

<sup>a</sup>Università degli Studi di Genova, via Dodecaneso 31, 16146 Genova, Italy. E-mail: diego.colombara@bath.edu

<sup>b</sup>Colorado School of Mines, 1301 19th St, Hill Hall, Golden, CO 80401, USA

<sup>c</sup>Università degli Studi di Parma, Parco Area delle Scienze, 181/A, 43124 Parma, Italy

† Revani is a traditional semolina-based Ottoman cake that is drenched with citrus syrup after baking. It is also known in Greece as *ravani*, in Egypt as *basbousa* and in Maghreb as *harissa hloua*.



Voltage losses in record cells have long been attributed to electrostatic potential fluctuations,<sup>14</sup> but SRH recombination cannot be excluded although it is hard to detect defects potentially acting as recombination centres.<sup>15</sup>

Voltage deficit in record CIGS has been shrinking since the introduction of alkali (Ak) metal doping in 1993. Ak metals are typically incorporated by diffusion of Na from soda-lime glass substrates and/or post-deposition treatments (Ak-PDT) performed on the absorber's surface after growth<sup>3,4</sup>. The beneficial effect of Ak-PDT on  $V_{OC}$  has been ascribed to reduced fluctuations,<sup>16</sup> decreased defect density at the interface,<sup>17</sup> and grain boundaries.<sup>18</sup> There is evidence that Ak-PDT reduces non-radiative recombination originating from grain boundaries,<sup>19</sup> also in combination with oxygen.<sup>20</sup> Yet, the underlying diffusion interplay between Ak dopants and matrix atoms in CIGS<sup>21–23</sup> (including its copper deficient surface layer, CDL<sup>24</sup>), cannot be excluded to play an important role within the interior of the grains, given that photoluminescence analyses point to Ak reducing electrostatic potential fluctuations even in CIGS free from grain boundaries.<sup>25</sup>

CIGS is a complex playground for exotic atomic diffusion phenomena that we are just now starting to grasp.<sup>26,27</sup> This contribution simplifies the picture with a wet sponge cake called *revani*, where the porous cake itself is the CIGS lattice and the wet syrup is the Ak metal dopant, particularly the sodium.

### 3. Revani model of atomic diffusion interdependence

This model (Fig. 1) is a simplification of a new theory of atomic diffusion illustrated in ref. 26 that is based on experimental evidence from Na-doped Cu(In,Ga)Se<sub>2</sub> (ref. 22 and 28) and is partially supported by a computational study.<sup>29</sup> Starting assumption for the theory is that diffusion of sodium can take place *via* both vacancy and interstitial sites, according to the known Frank–Turnbull mechanism (FT).<sup>30</sup> Although the FT mechanism has never been confirmed experimentally in CIGS,<sup>31</sup> its likelihood is supported implicitly by computational studies of atomic migration.<sup>32,33</sup>



Fig. 1 Revani model of atomic diffusion in CIGS. A dopant (e.g. Na, green) within CIGS may enhance (a) surface/boundary diffusivity (e.g. of another foreign atom like K, purple<sup>4</sup>) and/or (b) grain interior/bulk diffusivity (e.g. of matrix atoms like In, cyan<sup>22</sup>), if its own diffusion occurs *via* the Frank–Turnbull (FT) mechanism and is faster than those of foreign/matrix atoms in CIGS. The two red arrows in the middle section signify the FT mechanism of a Na atom diffusing to and from substitutional/interstitial sites.

In essence, the theory argues that the close proximity between atomic surfactants<sup>34,35</sup> (e.g. sodium dopant atoms) and matrix anions (selenium) lowers the bond strength between the matrix anions and the matrix cations (copper, indium and gallium), thus decreasing the energy barrier for atomic migration. The end result is a migration catalysis: the spatial distribution of matrix atoms in the material (*i.e.* from the atomic to the microscopic level) may more easily approach the thermodynamic limit by taking advantage of faster diffusion kinetics. This migration catalysis may take place, to different extents, at CIGS surfaces and grain boundaries (Fig. 1a) or grain interiors (Fig. 1b).

(a) Revani cake soaking stage, Fig. 1a. At interfaces and grain boundaries the presence of sodium can enhance ion exchange and induce incorporation of impurity atoms such as potassium and rubidium during AK-PDT.

(b) Revani cake squeezing stage, Fig. 1b. In the bulk of CIGS grains, sodium may ease the attainment of the equilibrium elemental distribution, *i.e.* the CIGS-OVC phase separation, with the latter destined to occupy surfaces and boundaries.

It follows from this model that the respective localization of sodium and other elements at CIGS interfaces, grain boundaries or interiors is highly interdependent.<sup>36</sup> The interdependence occurs because the migration route of sodium overlaps with the migration routes of the other elements, leading to mutually perturbed hopping events. The exact outcome of this interdependence originates from an interplay between process temperature and local composition (chemical potentials<sup>37</sup>), jointly dictating the concentration of point defects, the frequency of the event, and hence the likelihood of each individual jump in the presence of the thermodynamic driving force represented by phase segregation.

### 4. Fingerprints of the revani model from the literature

Since the dawn of CIGS research, it is known that film texture and grain size vary significantly, depending on the chemical composition during growth and especially on the presence or absence of Ak metal impurities. Ironically, crucial supporting hints come from the very first study on sodium doping dating back to 1993.<sup>38</sup> X-ray diffractograms of CIS films grown on soda-lime glass substrates showed pronounced crystallographic orientation such that “virtually no other peak than the (112)” was seen for uncoated substrates. The effect was confirmed by other groups worldwide<sup>39–41</sup> and linked to sodium incorporation, but the broader implications have been underappreciated. Interestingly, changes in preferred orientation from (112) to (220) were reported in the presence of sodium if the deposition temperature is increased up to 570 °C,<sup>42</sup> hinting to a transition temperature between diffusion regimes.

#### 4.1. Origin of anisotropy-induced fluctuations

If sodium diffusion occurs (also) through interstitials, as assumed in the *revani* model, different crystallographic orientation of the grains become a possible source of property



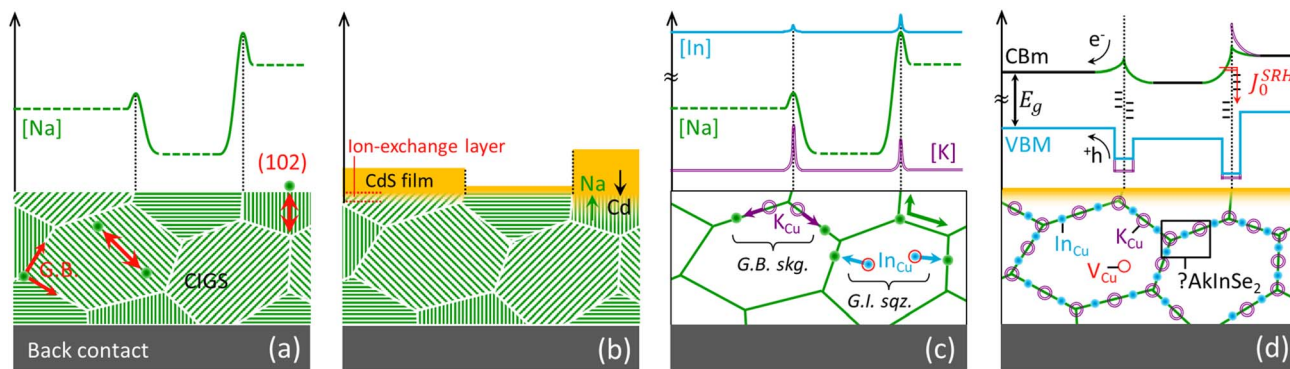


Fig. 2 Possible anisotropy-induced fluctuations caused by orientation-dependent diffusivity of sodium in CIGS, as simplified by the *revani* model. (a) If sodium diffuses *via* the FT mechanism, crystallographic directions displaying a larger concentration of interstitial sites (e.g. (220) and (102) shown by the red double arrows) will act as preferential pathways for sodium diffusion and for indium–gallium mass transport, as displayed here in a non-textured polycrystalline film. Hence, the growth of various grains is expected to be self-selected, leading to textured films with interstitial-poor (112) planes parallel to the sodium-containing substrate. Likewise, the concentration of sodium from one grain to another may vary as a result of orientation dependent uptake of extrinsic dopant, leading to granularity of carrier density at the length scale of grain size. (b) The preferential diffusion of sodium along certain crystallographic directions implies an effectively larger sodium availability for ion–exchange reactions at the surface of those grains oriented with (112) planes perpendicular to the substrate, such that it may affect buffer layer nucleation and growth when this is done by chemical bath deposition, as observed by Witte *et al.*<sup>48</sup> (c) *Revani* soaking (skg.) and squeezing (sqz.) stages, exemplified by uptake of potassium atoms at CIGS grain boundaries (GB) through ion exchange by sodium (both identified at G.B.<sup>49</sup>), and by removal of  $\text{In}_{\text{Cu}}$  donors from grain interior (GI) towards GBs. (d) Electronic consequences of the *revani* model onto the band structure of CIGS across GBs: bandgap widening at the GBs results from a lowering of the valence band maximum and a lift of the conduction band minimum following the compositional alterations. Such a band structure effectively repels photogenerated electron–hole pairs from defect-rich GB regions otherwise responsible for Shockley–Read–Hall recombination, as suggested by Keller *et al.*<sup>50</sup>

fluctuations at the microscale. In fact, grains with (220) or (102) planes oriented perpendicular to the substrate may convey a higher concentration of mobile  $\text{Na}^+$  cations, due to the higher concentration of interstitial sites they contain, compared to e.g. (112) oriented grains, as exemplified in Fig. 2a. Certain facets are expected to grow at a higher rate than others, due to higher orientation-dependent atomic diffusivity induced by sodium. The proposed FT-induced anisotropy of sodium migration in CIGS complements previous studies on spontaneous surface faceting<sup>43–46</sup> and is consistent with recent findings where preferential sodium diffusion was reported to occur through the (220)/(204) crystallographic direction.<sup>47</sup>

#### 4.2. Implications for doping density fluctuations

The model implies lateral step fluctuations of acceptor concentration. Even though the impact of these inhomogeneities on device performance appears negligible for highly efficient narrow-gap CIGS cells,<sup>51–53</sup> it may still be a problem for modules and wider gap CIGS.

#### 4.3. Implications for potential-induced degradation (PID)

Sodium diffusion is the most likely culprit for PID in CIGS, a module performance degradation that is common to all PV technologies.<sup>54</sup> PID occurs when a high voltage forms between the solar cells in the module and the module frame, notably when numerous modules are connected in series to attain a high voltage output while minimising resistance losses. In CIGS, sodium is thought to electromigrate and impair the p–n junction and/or corrode the TCO contact.<sup>55,56</sup> Granularity in the sodium accumulation was reported by Harvey *et al.*,<sup>57</sup>

suggesting preferential diffusion through certain grains that may be compatible with the *revani* model, even though the authors attribute the effect to grain boundary diffusion. The model may be tested experimentally by assessing the resilience to PID of cells whose CIGS absorber was deliberately grown with different preferential orientations.<sup>47</sup> It is worth noting that the main CIGS PV manufacturers have overcome PID issues by employing barriers that prevent sodium diffusion from substrate, and encapsulant glass slabs during operation.

#### 4.4. Implications for buffer thickness fluctuations

Different sodium availability from grain to grain, or facet to facet, would also lead to a different extent of ionic exchange *via* the *revani* model, as shown in Fig. 2b. This scenario is consistent with recent findings revealing that CdS and Zn(O,S) buffer growth by chemical bath deposition is impaired on as-formed (112) CIGS facets<sup>48,58</sup>, where sodium availability through the interstitial route is less likely. Although the effect may be due to other differences in surface energetics, the *revani* hypothesis should be tested.

#### 4.5. Implications for inter/intra-grain fluctuations

The soaking stage (Fig. 2c, G.B. skg.) accounts for the intake of heavier Ak atoms favoured over sodium,<sup>4,59–62</sup> which results in passivation due to bandgap widening at the grain boundary (Fig. 2d). Simulations have shown that even in the presence of high concentrations of defects at grain boundaries, the performance of the cell improves if the energy gap at the grain boundaries is sufficiently large compared to that of the grain interior.<sup>63</sup> The intake of heavier Ak ions may occur by



displacement of sodium ions (*i.e.* by exchange), or by a concerted movement of a sodium ion from its substitutional position to an interstitial site and concomitant incorporation of the heavier Ak ion into the emptied copper site (*i.e.* by FT mediation). This stage would also explain why a potassium-enriched surface is more prone to exchange potassium for cadmium, accounting for the improved CIGS/CdS heterojunction in K-doped films.<sup>4</sup>

The squeezing stage (Fig. 2c, G.I. sqz.) accounts for sodium-induced migration of  $\text{In}_{\text{Cu}}$  antisite donors to the grain boundaries, thus decreasing compensation in the bulk (increasing the relative share of copper vacancies in the grains<sup>64,65</sup>) and turning the boundaries indium-rich (adding to bandgap widening) at the same time. This could explain why Na-doping increases the net acceptor concentration in CIGS,<sup>66</sup> without excluding a concomitant increase of copper vacancies within the grains, according to the model by Yuan *et al.*<sup>67</sup> (Fig. 2d), which is supported by the recent detection of sparse Cu-rich GBs even in nominally Cu-poor films.<sup>68</sup>

The combined effect is consistent with the general decrease of electrostatic potential fluctuations and may explain why sodium doping happens to be essential in the first place. In 2018, highly efficient single crystal devices were obtained for the first time in the history of CIGS. Decisively, these were fabricated with epitaxial absorbers subject to NaF and KF-PDTs.<sup>69</sup> Such a fact demonstrates that good CIGS optoelectronic quality can indeed be attained even in the absence of grain boundaries, a conundrum that took many years to unravel!

## 5. Numerical simulations

Since the hypothesized fluctuations have a common root cause, we conduct numerical simulations at the device level to analyse how the varying thickness of the CdS buffer layer, along with the presence of fluctuating doping density in the underlying CIGS, affects the behaviour of the solar cell.

The cell is simulated with the Synopsys Sentaurus-TCAD suite. The current–voltage characteristics of the cell is calculated by solving the Poisson and continuity equations for electrons and holes in a coupled manner, using the drift–diffusion model, and incorporating the effects of non-radiative recombination in the various layers through the Shockley–Read–Hall model. The behavior of the illuminated cell is computed by illuminating it with the AM1.5G spectrum and employing the experimental complex refractive indices of the various layers for the calculation of optical generation and reflection.<sup>70,71</sup> The Transfer Matrix Method (TMM) is employed to analyze the behavior of the solar cells as the light passes through its layers. In each layer, the optical intensity is determined by evaluating the electric field amplitudes of both forward- and backward-propagating waves, considering the optical properties of the material, which are described by the complex refractive index. Afterwards, the optical generation is computed from the calculated optical intensity and wavelength-dependent absorption coefficient.

Fig. 3 depicts the two grains cell model following the standard configuration of CIGS cell, *i.e.*, from top to bottom,  $\text{MgF}_2$



Fig. 3 Schematic representation of the two-grains CIGS solar cell model (not to scale) employed to simulate the effects on device performance of anisotropy-induced fluctuations such as grain-dependent CdS buffer thickness and p-type doping.

anti-reflecting coating, Aluminum doped ZnO window, high-resistive ZnO, CdS buffer and CIGS absorber. In particular, in grain A, the thickness of CdS, and the doping of the underlying CIGS are fixed and set at 40 nm and  $10^{16} \text{ cm}^{-3}$ , respectively, while in grain B, they can vary. Similar to the ZSW cell, we also consider a  $\text{MgF}_2$  antireflective coating with a thickness of 100 nm to reduce reflection at the cell surface. We simulated the two-dimensional cross section of the cell in the red frame.

The main properties of the different layers and interfaces used in the simulation are summarized in Table 1. More details about simulations and material parameters can be found in our previous works.<sup>72</sup>

First and foremost, we simulate a reference cell characterized by a constant buffer layer thickness and uniform CIGS doping throughout the grains, *i.e.*, same  $t_{\text{CdS}} = 40 \text{ nm}$ , and acceptor density  $N_{\text{A}} = 10^{16} \text{ cm}^{-3}$  in both grain A and B, replicating a ZSW cell with an efficiency > 22%.<sup>3</sup>

The ZSW cell features a double-graded  $[\text{Ga}]/([\text{Ga}] + [\text{In}])$  (GGI) composition CIGS layer, so we include the measured GGI profile

Table 1 Main parameters used in the simulations.<sup>72</sup> The CdS thickness and p-type doping in CIGS grain A are set at 40 nm and  $10^{16} \text{ cm}^{-3}$ , respectively, whereas in grain B they are subject to variation. See Fig. 3 and text for more details

	AZO	i-ZnO	CdS	CIGS
$E_{\text{g}}/\text{eV}$	3.3	3.3	2.4	Graded
Thickness/nm	200	50	40 nm/variable	2300
Doping/ $\text{cm}^{-3}$	$5 \times 10^{19}$	$10^{17}$	$10^{17}$	$10^{16}$ /variable
$\mu_{\text{e}} (\mu_{\text{h}})/\text{cm}^2 \text{ V}^{-1} \text{ s}^{-1}$	100 (25)			
$\tau_{\text{e}} (\tau_{\text{h}})/\text{ns}$	10 (0.01)	10 (0.01)	33 (0.01)	250 (250)
CBO/eV	−0.2		0.1	



**Table 2** Comparison between CIGS solar cell parameters for a real device fabricated by ZSW,<sup>3</sup> and the closely matching numerical simulation constituting the base for the simulations performed here (reference cell)

	$V_{oc}/V$	$J_{sc}/\text{mA cm}^{-2}$	ff/%	$\eta/\%$
ZSW	0.744	36.70	80.50	22.00
Simulation	0.744	36.75	80.53	22.03

of the highest efficiency cell shown in <sup>73</sup> within the CIGS layer. This allows to account for the varying bandgap grading in the CIGS layer and related optical coefficients that depend on the GGI and position, as illustrated in <sup>74</sup>. The IV curve is also influenced by the alignment of the conduction bands at the hetero-interfaces, as shown in <sup>75</sup>. In our simulations, we have considered a conduction band offsets (CBO) of 0.1 eV, creating a spike (*i.e.*, the conduction band at the CIGS side is lower than that at the CdS side) at the CdS/CIGS interface, and 0.2 eV, forming a cliff (*i.e.*, the conduction band at the ZnO side is lower than that at the CdS side) at the ZnO/CdS interface.

Furthermore, we assume ideal heterointerfaces, which entails zero recombination velocity. This choice was made to direct our attention specifically towards assessing the impact of variations of doping and CdS thickness on cell performance.

The parameters of the simulated reference cell closely match those of the 22% efficient CIGS cell fabricated by ZSW, as summarised in Table 2.

To examine how changes in the CdS thickness and doping levels within the CIGS layer might affect the cell's performance, our approach simulates two grains of the cell (*cf.* Fig. 3): in grain A, we maintain a uniform CdS thickness of 40 nm and CIGS doping density of  $10^{16} \text{ cm}^{-3}$ , as in the reference cell. In grain B, we set either a CdS thickness  $t_{\text{CdS}} = 30 \text{ nm}$  with a CIGS doping density,  $N_A$ , ranging between  $10^{15} \text{ cm}^{-3}$  and  $10^{16} \text{ cm}^{-3}$  (referred to as "scenario I"), or  $t_{\text{CdS}} = 50 \text{ nm}$  with  $N_A$  ranging from  $10^{16} \text{ cm}^{-3}$  to  $10^{17} \text{ cm}^{-3}$  (denoted as "scenario II").

Moreover, to determine if the impact of inhomogeneities can vary with grain size, simulations were performed for each combination of  $t_{\text{CdS}}$  and  $N_A$  using three different grain sizes,  $d_G$ , of 0.25  $\mu\text{m}$ , 0.5  $\mu\text{m}$ , and 1  $\mu\text{m}$ .

Fig. 4 shows the results of numerical simulations performed with varying  $t_{\text{CdS}}$  against the CIGS doping level in grain B,  $N_A$ , with each distinct curve corresponding to different grain sizes (denoted as  $d_G$ ). Each plot can be divided into two distinct regions: region I displays findings corresponding to scenario I, while region II presents results from scenario II.

The cell parameters of the reference cell, characterized by grains with uniform CdS thickness of 40 nm and CIGS doping of  $10^{16} \text{ cm}^{-3}$ , are represented by the star symbol and are positioned midway between region I and region II.

Concerning the trends exhibited by the simulated cell parameters, the observed behaviours stem from a combination of electrical and optical factors.

Specifically, an increased thickness of the CdS layer decreases charge carrier generation within the CIGS layer, consequently affecting  $J_{sc}$ .



**Fig. 4** Simulated solar cell parameters for the solar cell sketched in Fig. 3. In all simulations, grain A has a uniform CdS thickness of 40 nm and CIGS doping density of  $10^{16} \text{ cm}^{-3}$  (star symbol in the figures). Region I displays results for the cell in which grain B has  $t_{\text{CdS}} = 30 \text{ nm}$  and variable CIGS doping density ( $10^{15} \text{ cm}^{-3} \leq N_A \leq 10^{16} \text{ cm}^{-3}$ ); region II displays results for the cell in which grain B has  $t_{\text{CdS}} = 50 \text{ nm}$  and variable CIGS doping density ( $10^{16} \text{ cm}^{-3} \leq N_A \leq 10^{17} \text{ cm}^{-3}$ ). Different curves represent grain sizes with dimensions  $d_G = 0.25, 0.5, 1 \mu\text{m}$  (square, circle, triangle symbols).



This phenomenon is readily apparent in Fig. 4b for a doping level in grain B set at  $N_A = 10^{16} \text{ cm}^{-3}$ : in this case,  $J_{SC}$  exhibits the highest current value at  $t_{CDS} = 30 \text{ nm}$  while a lower value is observed at  $t_{CDS} = 50 \text{ nm}$ .

Conversely, a higher doping level in the CIGS layer enhances  $V_{OC}$  by reducing non-radiative recombination processes (Fig. 4a), also enhancing  $J_{SC}$  (Fig. 4b).

As a result of the combined influence of these factors, the cell efficiency curve exhibits a variation of over 1% in absolute efficiency, with a more pronounced impact observed in the case of larger grain sizes,  $d_G$ .

The relationship between grain size and efficiency variation suggests that the portion of the grain with doping and CIGS thickness deviations has a greater influence compared to the portion with expected values.

If we visualize a cell containing thousands of grains resembling the ones being simulated, the simulations indicate that these deviations have a growing significance when dealing with larger grains and areas of non-uniformity that are similar to the homogeneous regions.

## 6. Conclusions

The evolution of CIGS solar cell performance over the years can be traced back to key technological innovations that improved the absorber's optoelectronic properties. Among these, Ak metal doping—especially sodium—has undeniably played the lion's share to success. Here, a *revani* (wet sponge cake) model of atomic diffusion, with soaking and squeezing stages, is proposed as a simple unifying concept to account for a number of unsettled experimental facts. The proposed micro-scale anisotropy-induced fluctuations, if confirmed, may account for bandgap tailing and voltage deficit in CIGS cells and/or modules. We encourage the community to test these hypotheses.

## Conflicts of interest

There are no conflicts of interest to declare.

## Acknowledgements

DC wishes to thank the organisers and attendees of the 49<sup>th</sup> IEEE Photovoltaics Specialists Conference (PVSC) held in June 2022 in Philadelphia for their interest on an earlier version of this study<sup>76</sup> and for fruitful discussions. We would like to thank Susanne Siebentritt (U. of Luxembourg), Hossam Elanzeery (Avancis GmbH), Nicoleta Nicoara and Sascha Sadewasser (INL, Portugal), Luis Pazos-Outón (Google Inc.), Stefano Rampino, Edmondo Gilioli, and Massimo Mazzer (CNR IMEM, Italy) for valuable discussions. This research was funded by the University of Genova and Compagnia di San Paolo through the Curiosity Driven and Promoting Competitiveness schemes, and by the Italian Ministry of University and Research through the LEGACY (healing wide-gap chalcopyrite, grant No. 20223ZP4WP) project of national relevance (PRIN 2022), under the PE3 Condensed Matter Physics sector.

## References

- 1 M. A. Green, *et al.*, Solar cell efficiency tables (version 62), *Prog. Photovolt.: Res. Appl.*, 2023, **31**(7), 651–663, DOI: [10.1002/pip.3726](https://doi.org/10.1002/pip.3726).
- 2 M. Nakamura, K. Yamaguchi, Y. Kimoto, Y. Yasaki, T. Kato and H. Sugimoto, Cd-Free Cu(In,Ga)(Se,S)<sub>2</sub> Thin-Film Solar Cell With Record Efficiency of 23.35, *IEEE J. Photovolt.*, 2019, **9**(6), 1863–1867, DOI: [10.1109/JPHOTOV.2019.2937218](https://doi.org/10.1109/JPHOTOV.2019.2937218).
- 3 P. Jackson, R. Wuerz, D. Hariskos, E. Lotter, W. Witte and M. Powalla, Effects of heavy alkali elements in Cu(In,Ga)Se<sub>2</sub> solar cells with efficiencies up to 22.6, *Phys Status Solidi Rapid Res Lett.*, 2016, **10**(8), 583–586, DOI: [10.1002/pssr.201600199](https://doi.org/10.1002/pssr.201600199).
- 4 A. Chirilă, *et al.*, Potassium-induced surface modification of Cu(In,Ga)Se<sub>2</sub> thin films for high-efficiency solar cells, *Nat. Mater.*, 2013, **12**(12), 1107–1111, DOI: [10.1038/nmat3789](https://doi.org/10.1038/nmat3789).
- 5 M. Jošt, *et al.*, 21.6%-Efficient Monolithic Perovskite/Cu(In,Ga)Se<sub>2</sub> Tandem Solar Cells with Thin Conformal Hole Transport Layers for Integration on Rough Bottom Cell Surfaces, *ACS Energy Lett.*, 2019, **4**(2), 583–590, DOI: [10.1021/acsenerylett.9b00135](https://doi.org/10.1021/acsenerylett.9b00135).
- 6 V. Bermudez and A. Perez-Rodriguez, Understanding the cell-to-module efficiency gap in Cu(In,Ga)(S,Se)<sub>2</sub> photovoltaics scale-up, *Nat. Energy*, 2018, **3**(6), 466–475, DOI: [10.1038/s41560-018-0177-1](https://doi.org/10.1038/s41560-018-0177-1).
- 7 M. A. Contreras, *et al.*, Wide bandgap Cu(In,Ga)Se<sub>2</sub> solar cells with improved energy conversion efficiency, *Prog. Photovolt.: Res. Appl.*, 2012, **20**(7), 843–850, DOI: [10.1002/pip.2244](https://doi.org/10.1002/pip.2244).
- 8 F. Larsson, *et al.*, Record 1.0 V open-circuit voltage in wide band gap chalcopyrite solar cells, *Prog. Photovolt.: Res. Appl.*, 2017, **25**(9), 755–763, DOI: [10.1002/pip.2914](https://doi.org/10.1002/pip.2914).
- 9 M. Sood, *et al.*, Passivating Surface Defects and Reducing Interface Recombination in CuInS<sub>2</sub> Solar Cells by a Facile Solution Treatment, *Sol. RRL*, 2021, **5**(4), 2100078, DOI: [10.1002/solr.202100078](https://doi.org/10.1002/solr.202100078).
- 10 S. Shukla, *et al.*, Carrier recombination mechanism and photovoltage deficit in 1.7-eV band gap near-stoichiometric Cu(In,Ga)S<sub>2</sub>, *Phys. Rev. Mater.*, 2021, **5**(5), 055403, DOI: [10.1103/PhysRevMaterials.5.055403](https://doi.org/10.1103/PhysRevMaterials.5.055403).
- 11 T. Nishimura, A. Doi, J. Chantana, A. Mavlonov, Y. Kawano and T. Minemoto, Silver-alloyed wide-gap CuGaSe<sub>2</sub> solar cells, *Sol. Energy*, 2021, **230**, 509–514, DOI: [10.1016/j.solener.2021.10.055](https://doi.org/10.1016/j.solener.2021.10.055).
- 12 S. Ishizuka, CuGaSe<sub>2</sub> Thin Film Solar Cells: Challenges for Developing Highly Efficient Wide-Gap Chalcopyrite Photovoltaics, *Phys. Status Solidi A*, 2019, **216**(15), 1800873, DOI: [10.1002/pssa.201800873](https://doi.org/10.1002/pssa.201800873).
- 13 A. Polman, M. Knight, E. C. Garnett, B. Ehrler and W. C. Sinke, Photovoltaic materials: Present efficiencies and future challenges, *Science*, 2016, **352**(6283), aad4424, DOI: [10.1126/science.aad4424](https://doi.org/10.1126/science.aad4424).



- 14 S. Siebentritt, What limits the efficiency of chalcopyrite solar cells?, *Sol. Energy Mater. Sol. Cells*, 2011, **95**(6), 1471–1476, DOI: [10.1016/j.solmat.2010.12.014](https://doi.org/10.1016/j.solmat.2010.12.014).
- 15 F. Werner, *et al.*, Alkali treatments of Cu(In,Ga)Se<sub>2</sub> thin-film absorbers and their impact on transport barriers, *Prog. Photovolt.: Res. Appl.*, 2018, **26**(11), 911–923, DOI: [10.1002/pip.3032](https://doi.org/10.1002/pip.3032).
- 16 S. A. Jensen, *et al.*, Beneficial effect of post-deposition treatment in high-efficiency Cu(In,Ga)Se<sub>2</sub> solar cells through reduced potential fluctuations, *J. Appl. Phys.*, 2016, **120**(6), 063106, DOI: [10.1063/1.4960344](https://doi.org/10.1063/1.4960344).
- 17 K. F. Tai, R. Kamada, T. Yagioka, T. Kato and H. Sugimoto, From 20.9 to 22.3% Cu(In,Ga)(S,Se)<sub>2</sub> solar cell: Reduced recombination rate at the heterojunction and the depletion region due to K-treatment, *Jpn. J. Appl. Phys.*, 2017, **56**(8S2), 08MC03, DOI: [10.7567/JJAP.56.08MC03](https://doi.org/10.7567/JJAP.56.08MC03).
- 18 S. Karki, P. Paul, G. Rajan, A. Rockett, A. Arehart and S. Marsillac, Characterization of Electronic Defects in RbF Treated CIGS Solar Cells, *Presented at the 7th World Conference on Photovoltaic Energy Conversion*, IEEE, Waikoloa, 2018.
- 19 S. Siebentritt, *et al.*, Heavy Alkali Treatment of Cu(In,Ga)Se<sub>2</sub> Solar Cells: Surface versus Bulk Effects, *Adv. Energy Mater.*, 2020, **10**(8), 1903752, DOI: [10.1002/aenm.201903752](https://doi.org/10.1002/aenm.201903752).
- 20 F. Babbe, *et al.*, Vacuum-Healing of Grain Boundaries in Sodium-Doped CuInSe<sub>2</sub> Solar Cell Absorbers, *Adv. Energy Mater.*, 2023, **13**(17), 2204183, DOI: [10.1002/aenm.202204183](https://doi.org/10.1002/aenm.202204183).
- 21 H. Rodriguez-Alvarez, *et al.*, Real-time study of Ga diffusion processes during the formation of Cu(In,Ga)Se<sub>2</sub>: The role of Cu and Na content, *Sol. Energy Mater. Sol. Cells*, 2013, **116**, 102–109, DOI: [10.1016/j.solmat.2013.04.008](https://doi.org/10.1016/j.solmat.2013.04.008).
- 22 D. Colombara, *et al.*, Sodium enhances indium-gallium interdiffusion in copper indium gallium diselenide, *Nat. Commun.*, 2018, **9**, 826, DOI: [10.1038/s41467-018-03115-0](https://doi.org/10.1038/s41467-018-03115-0).
- 23 S. Zahedi-Azad, M. Maiberg and R. Scheer, Effect of Na-PDT and KF-PDT on the photovoltaic performance of wide bandgap Cu (In,Ga)Se<sub>2</sub> solar cells, *Prog. Photovolt.: Res. Appl.*, 2020, **28**(11), 1146–1157, DOI: [10.1002/pip.3317](https://doi.org/10.1002/pip.3317).
- 24 S. Ishizuka and P. J. Fons, Role of the Cu-Deficient Interface in Cu(In,Ga)Se<sub>2</sub> Thin-Film Photovoltaics with Alkali-Metal Doping, *Phys. Rev. Appl.*, 2021, **15**(5), 054005, DOI: [10.1103/PhysRevApplied.15.054005](https://doi.org/10.1103/PhysRevApplied.15.054005).
- 25 O. Ramirez, *et al.*, On the Origin of Tail States and Open Circuit Voltage Losses in Cu(In,Ga)Se<sub>2</sub>, *Sol. RRL*, 2023, **7**(13), 2300054, DOI: [10.1002/solr.202300054](https://doi.org/10.1002/solr.202300054).
- 26 D. Colombara, Frank-Turnbull dopant migration may enhance heteroatom diffusivity: Evidence from alkali-doped Cu(In,Ga)Se<sub>2</sub>, *Phys. Rev. Mater.*, 2019, **3**(5), 054602, DOI: [10.1103/PhysRevMaterials.3.054602](https://doi.org/10.1103/PhysRevMaterials.3.054602).
- 27 J. A. Grovogui, T. J. Slade, S. Hao, C. Wolverton, M. G. Kanatzidis and V. P. Dravid, Implications of doping on microstructure, processing, and thermoelectric performance: The case of PbSe, *J. Mater. Res.*, 2021, **36**(6), 1272–1284, DOI: [10.1557/s43578-021-00130-8](https://doi.org/10.1557/s43578-021-00130-8).
- 28 D. Colombara, *et al.*, Deliberate and Accidental Gas-Phase Alkali Doping of Chalcogenide Semiconductors: Cu(In,Ga)Se<sub>2</sub>, *Sci. Rep.*, 2017, **7**, 43266, DOI: [10.1038/srep43266](https://doi.org/10.1038/srep43266).
- 29 D. Colombara, K. Conley, M. Malitckaya, H.-P. Komsa and M. J. Puska, The fox and the hound: in-depth and in-grain Na doping and Ga grading in Cu(In,Ga)Se<sub>2</sub> solar cells, *J. Mater. Chem. A*, 2020, **8**(14), 6471–6479, DOI: [10.1039/D0TA01103G](https://doi.org/10.1039/D0TA01103G).
- 30 F. C. Frank and D. Turnbull, Mechanism of Diffusion of Copper in Germanium, *Phys. Rev.*, 1956, **104**(3), 617–618, DOI: [10.1103/PhysRev.104.617](https://doi.org/10.1103/PhysRev.104.617).
- 31 R. V. Forest, *et al.*, Diffusion of sodium in single crystal CuInSe<sub>2</sub>, *J. Appl. Phys.*, 2017, **121**(24), 245102, DOI: [10.1063/1.4986635](https://doi.org/10.1063/1.4986635).
- 32 L. E. Oikkonen, M. G. Ganchenkova, A. P. Seitsonen and R. M. Nieminen, Effect of sodium incorporation into CuInSe<sub>2</sub> from first principles, *J. Appl. Phys.*, 2013, **114**(8), 083503, DOI: [10.1063/1.4819105](https://doi.org/10.1063/1.4819105).
- 33 M. Malitckaya, H.-P. Komsa, V. Havu and M. J. Puska, Effect of Alkali Metal Atom Doping on the CuInSe<sub>2</sub>-Based Solar Cell Absorber, *J. Phys. Chem. C*, 2017, **121**(29), 15516–15528, DOI: [10.1021/acs.jpcc.7b03083](https://doi.org/10.1021/acs.jpcc.7b03083).
- 34 B. J. Stanbery, D. Abou-Ras, A. Yamada and L. Mansfield, CIGS photovoltaics: reviewing an evolving paradigm, *J. Phys. D: Appl. Phys.*, 2021, **55**(17), 173001, DOI: [10.1088/1361-6463/ac4363](https://doi.org/10.1088/1361-6463/ac4363).
- 35 B. J. Stanbery and *et al.*, Role of sodium in the control of defect structures in CIS [solar cells], in *Conference Record of the Twenty-Eighth IEEE Photovoltaic Specialists Conference*, Anchorage, AK, USA, 2000, pp. 440–445, DOI: [10.1109/PVSC.2000.915864](https://doi.org/10.1109/PVSC.2000.915864).
- 36 C. P. Muzzillo, Review of grain interior, grain boundary, and interface effects of K in CIGS solar cells: Mechanisms for performance enhancement, *Sol. Energy Mater. Sol. Cells*, 2017, **172**, 18–24, DOI: [10.1016/j.solmat.2017.07.006](https://doi.org/10.1016/j.solmat.2017.07.006).
- 37 D. Colombara, *et al.*, Chemical instability at chalcogenide surfaces impacts chalcopyrite devices well beyond the surface, *Nat. Commun.*, 2020, **11**(1), 3634, DOI: [10.1038/s41467-020-17434-8](https://doi.org/10.1038/s41467-020-17434-8).
- 38 J. Hedström and *et al.*, ZnO/CdS/Cu(In,Ga)Se<sub>2</sub> thin film solar cells with improved performance, *Presented at the Photovoltaic Specialists Conference, 1993. Conference Record of the Twenty Third IEEE*, IEEE, Louisville, KY, USA, 1993, pp. 364–371, DOI: [10.1109/pvsc.1993.347154](https://doi.org/10.1109/pvsc.1993.347154).
- 39 S. Ishizuka, *et al.*, Na-induced variations in the structural, optical, and electrical properties of Cu(In,Ga)Se<sub>2</sub> thin films, *J. Appl. Phys.*, 2009, **106**(3), 034908, DOI: [10.1063/1.3190528](https://doi.org/10.1063/1.3190528).
- 40 R. Sakdanuphab, C. Chityuttakan, A. Pankiew, N. Somwang, K. Yodee and S. Chatrathorn, Growth characteristics of Cu(In,Ga)Se<sub>2</sub> thin films using 3-stage deposition process with a NaF precursor, *J. Cryst. Growth*, 2011, **319**(1), 44–48, DOI: [10.1016/j.jcrysgro.2011.01.077](https://doi.org/10.1016/j.jcrysgro.2011.01.077).
- 41 B. J. Babu, S. Velumani, B. J. Simonds, R. K. Ahrenkiel, A. Kassiba and R. Asomoza, Effect of sodium doping on graded Cu(In<sub>1-x</sub>Ga<sub>x</sub>)Se<sub>2</sub> thin films prepared by chemical



- spray pyrolysis, *Mater. Sci. Semicond. Process.*, 2015, **37**, 37–45, DOI: [10.1016/j.mssp.2015.01.002](https://doi.org/10.1016/j.mssp.2015.01.002).
- 42 S.-R. Park, J.-Y. Baek, T.-Y. Yun, H.-J. Han, K.-B. Kim and C.-W. Jeon, Effect of Substrate Temperature on Preferred Orientation and Ga Composition Profile of Co-Evaporated Cu(In,Ga)Se<sub>2</sub>, *Mol. Cryst. Liq. Cryst.*, 2013, **585**(1), 114–120, DOI: [10.1080/15421406.2013.850941](https://doi.org/10.1080/15421406.2013.850941).
- 43 J. E. Jaffe and A. Zunger, Defect-induced nonpolar-to-polar transition at the surface of chalcopyrite semiconductors, *Phys. Rev. B*, 2001, **64**(24), 241304, DOI: [10.1103/PhysRevB.64.241304](https://doi.org/10.1103/PhysRevB.64.241304).
- 44 D. Liao and A. Rockett, Epitaxial growth of Cu(In, Ga)Se<sub>2</sub> on GaAs(110), *J. Appl. Phys.*, 2002, **91**(4), 1978–1983, DOI: [10.1063/1.1434549](https://doi.org/10.1063/1.1434549).
- 45 Y. Hinuma, F. Oba, Y. Kumagai and I. Tanaka, Ionization potentials of (112) and (112) facet surfaces of CuInSe<sub>2</sub> and CuGaSe<sub>2</sub>, *Phys. Rev. B*, 2012, **86**(24), 245433, DOI: [10.1103/PhysRevB.86.245433](https://doi.org/10.1103/PhysRevB.86.245433).
- 46 A. Shigemi and T. Wada, Surface Stabilities of Various Crystal Faces of CuInSe<sub>2</sub> and Related Compounds by First-Principles Calculation, *Jpn. J. Appl. Phys.*, 2012, **51**(10S), 10NC22, DOI: [10.1143/JJAP.51.10NC22](https://doi.org/10.1143/JJAP.51.10NC22).
- 47 T.-Y. Lin, C.-H. Chen, L.-W. Wang, W.-C. Huang, Y.-W. Jheng and C.-H. Lai, Engineering Na-transport to achieve high efficiency in ultrathin Cu(In,Ga)Se<sub>2</sub> solar cells with controlled preferred orientation, *Nano Energy*, 2017, **41**, 697–705.
- 48 W. Witte, D. Abou-Ras and D. Hariskos, Improved growth of solution-deposited thin films on polycrystalline Cu(In,Ga)Se<sub>2</sub>, *Phys Status Solidi Rapid Res Lett.*, 2016, **10**(4), 300–304, DOI: [10.1002/pssr.201510454](https://doi.org/10.1002/pssr.201510454).
- 49 O. Cojocar-Mirédin, T. Schwarz and D. Abou-Ras, Assessment of elemental distributions at line and planar defects in Cu(In,Ga)Se<sub>2</sub> thin films by atom probe tomography, *Scr. Mater.*, 2018, **148**, 106–114, DOI: [10.1016/j.scriptamat.2017.03.034](https://doi.org/10.1016/j.scriptamat.2017.03.034).
- 50 D. Keller, *et al.*, Band gap widening at random CIGS grain boundary detected by valence electron energy loss spectroscopy, *Appl. Phys. Lett.*, 2016, **109**(15), 153103, DOI: [10.1063/1.4964516](https://doi.org/10.1063/1.4964516).
- 51 D. Abou-Ras, N. Schäfer, C. J. Hages, S. Levchenko, J. Márquez and T. Unold, Inhomogeneities in Cu(In,Ga)Se<sub>2</sub> Thin Films for Solar Cells: Band-Gap Versus Potential Fluctuations, *Sol. RRL*, 2018, **2**(1), 1700199, DOI: [10.1002/solr.201700199](https://doi.org/10.1002/solr.201700199).
- 52 M. Krause, A. Nikolaeva, P. Jackson, D. Hariskos, W. Witte, and D. Abou-Ras, “Microscopic Materials Properties of a High-Efficiency Cu(In,Ga)Se<sub>2</sub> Solar Cell - a Case Study,” *Presented at the 7th World Conference on Photovoltaic Energy Conversion*, Waikoloa, 2018.
- 53 M. Krause, *et al.*, Microscopic origins of performance losses in highly efficient Cu(In,Ga)Se<sub>2</sub> thin-film solar cells, *Nat. Commun.*, 2020, **11**(1), DOI: [10.1038/s41467-020-17507-8](https://doi.org/10.1038/s41467-020-17507-8).
- 54 P. Yilmaz, J. Schmitz and M. Theelen, Potential induced degradation of CIGS PV systems: A literature review, *Renewable Sustainable Energy Rev.*, 2022, **154**, 111819, DOI: [10.1016/j.rser.2021.111819](https://doi.org/10.1016/j.rser.2021.111819).
- 55 V. Fjällström, *et al.*, Potential-Induced Degradation of CuIn<sub>1-x</sub>Ga<sub>x</sub>Se<sub>2</sub> Thin Film Solar Cells, *IEEE J. Photovolt.*, 2013, **3**(3), 1090–1094, DOI: [10.1109/JPHOTOV.2013.2253833](https://doi.org/10.1109/JPHOTOV.2013.2253833).
- 56 C. P. Muzzillo, *et al.*, Potential-Induced Degradation of Cu(In,Ga)Se<sub>2</sub> Solar Cells: Alkali Metal Drift and Diffusion Effects, *IEEE J. Photovolt.*, 2018, **8**(5), 1337–1342, DOI: [10.1109/JPHOTOV.2018.2858549](https://doi.org/10.1109/JPHOTOV.2018.2858549).
- 57 S. P. Harvey, *et al.*, Investigating PID Shunting in Polycrystalline CIGS Devices via Multi-Scale, Multi-Technique Characterization, *IEEE J. Photovolt.*, 2019, **9**(2), 559–564, DOI: [10.1109/JPHOTOV.2019.2892874](https://doi.org/10.1109/JPHOTOV.2019.2892874).
- 58 W. Witte, D. Abou-Ras and D. Hariskos, Chemical bath deposition of Zn(O,S) and CdS buffers: Influence of Cu(In,Ga)Se<sub>2</sub> grain orientation, *Appl. Phys. Lett.*, 2013, **102**(5), 051607, DOI: [10.1063/1.4788717](https://doi.org/10.1063/1.4788717).
- 59 L. Stolt, E. Wallin, S. Soderger, T. Jarmar and M. Edoff, “Alkali Element Interdependence in CIGS Relating to Depth Distribution of Na/K and Ga/(Ga+In),” *Presented at the Materials Research Society Meeting*, Phoenix, 2017. [Online]. Available: <https://mrsspring.zerista.com/event/member/363893>.
- 60 O. Donzel-Gargand, *et al.*, Deep surface Cu depletion induced by K in high-efficiency Cu(In,Ga)Se<sub>2</sub> solar cell absorbers, *Prog. Photovolt.: Res. Appl.*, 2018, **26**(9), 730, DOI: [10.1002/pip.3010](https://doi.org/10.1002/pip.3010).
- 61 A. Vilalta-Clemente, *et al.*, Rubidium distribution at atomic scale in high efficient Cu(In,Ga)Se<sub>2</sub> thin-film solar cells, *Appl. Phys. Lett.*, 2018, **112**(10), 103105, DOI: [10.1063/1.5020805](https://doi.org/10.1063/1.5020805).
- 62 T. Bertram and *et al.*, RbF-PDT induced sodium displacement in Cu(In, Ga)Se<sub>2</sub> Absorbers Grown under High Substrate Temperatures,” *Presented at the 7th World Conference on Photovoltaic Energy Conversion*, Waikoloa, 2018.
- 63 G. Sozzi, O. Cojocar-Mirédin, and R. Wuerz, A simulation study on the effect of sodium on grain boundary passivation in CIGS thin-film solar cells, in *2021 IEEE 48th Photovoltaic Specialists Conference (PVSC)*, 2021, pp. 0187–0191, DOI: [10.1109/PVSC43889.2021.9518887](https://doi.org/10.1109/PVSC43889.2021.9518887).
- 64 D. Abou-Ras, *et al.*, Compositional and electrical properties of line and planar defects in Cu(In,Ga)Se<sub>2</sub> thin films for solar cells – a review, *Phys Status Solidi Rapid Res Lett.*, 2016, **10**(5), 363–375, DOI: [10.1002/pssr.201510440](https://doi.org/10.1002/pssr.201510440).
- 65 C. Stephan, D. Greiner, S. Schorr and C. A. Kaufmann, The influence of sodium on the point defect characteristics in off stoichiometric CuInSe<sub>2</sub>, *J. Phys. Chem. Solids*, 2016, **98**, 309–315, DOI: [10.1016/j.jpcs.2016.07.022](https://doi.org/10.1016/j.jpcs.2016.07.022).
- 66 S.-H. Wei, S. B. Zhang and A. Zunger, Effects of Na on the electrical and structural properties of CuInSe<sub>2</sub>, *J. Appl. Phys.*, 1999, **85**(10), 7214–7218, DOI: [10.1063/1.370534](https://doi.org/10.1063/1.370534).
- 67 Z. Yuan, *et al.*, Na-Diffusion Enhanced p-type Conductivity in Cu(In,Ga)Se<sub>2</sub>: A New Mechanism for Efficient Doping in Semiconductors, *Adv. Energy Mater.*, 2016, **6**(24), 1601191, DOI: [10.1002/aenm.201601191](https://doi.org/10.1002/aenm.201601191).
- 68 M. Raghuwanshi, *et al.*, Fingerprints Indicating Superior Properties of Internal Interfaces in Cu(In,Ga)Se<sub>2</sub> Thin-Film



- Solar Cells, *Adv. Mater.*, 2022, **34**(37), 2203954, DOI: [10.1002/adma.202203954](https://doi.org/10.1002/adma.202203954).
- 69 J. Nishinaga, T. Nagai, T. Sugaya, H. Shibata and S. Niki, Single-crystal Cu(In,Ga)Se<sub>2</sub> solar cells grown on GaAs substrates, *Appl. Phys. Express*, 2018, **11**(8), 082302, DOI: [10.7567/APEX.11.082302](https://doi.org/10.7567/APEX.11.082302).
- 70 R. Carron, *et al.*, Refractive indices of layers and optical simulations of Cu(In,Ga)Se<sub>2</sub> solar cells, *Sci. Technol. Adv. Mater.*, 2018, **19**(1), 396–410, DOI: [10.1080/14686996.2018.1458579](https://doi.org/10.1080/14686996.2018.1458579).
- 71 T. Hara, T. Maekawa, S. Minoura, Y. Sago, S. Niki and H. Fujiwara, Quantitative Assessment of Optical Gain and Loss in Submicron-Textured CuIn<sub>1-x</sub>Ga<sub>x</sub>Se<sub>2</sub> Solar Cells Fabricated by Three-Stage Coevaporation, *Phys. Rev. Appl.*, 2014, **2**(3), 034012, DOI: [10.1103/PhysRevApplied.2.034012](https://doi.org/10.1103/PhysRevApplied.2.034012).
- 72 G. Sozzi, S. Di Napoli, R. Menozzi, B. Bissig, S. Buecheler and A. N. Tiwari, Impact of front-side point contact/passivation geometry on thin-film solar cell performance, *Sol. Energy Mater. Sol. Cells*, 2017, **165**, 94–102, DOI: [10.1016/j.solmat.2017.02.031](https://doi.org/10.1016/j.solmat.2017.02.031).
- 73 P. Jackson, *et al.*, Properties of Cu(In,Ga)Se<sub>2</sub> solar cells with new record efficiencies up to 21.7, *Phys Status Solidi Rapid Res Lett.*, 2015, **9**(1), 28–31, DOI: [10.1002/pssr.201409520](https://doi.org/10.1002/pssr.201409520).
- 74 G. Sozzi and *et al.*, Analysis of Ga grading in CIGS absorbers with different Cu content, in *2016 IEEE 43rd Photovoltaic Specialists Conference (PVSC)*, 2016, pp. 2279–2282, DOI: [10.1109/PVSC.2016.7750042](https://doi.org/10.1109/PVSC.2016.7750042).
- 75 G. Sozzi and *et al.*, Influence of Conduction Band Offsets at Window/Buffer and Buffer/Absorber Interfaces on the Roll-Over of J-V Curves of CIGS Solar Cells, in *2017 IEEE 44th Photovoltaic Specialist Conference (PVSC)*, 2017, pp. 2205–2208, DOI: [10.1109/PVSC.2017.8366649](https://doi.org/10.1109/PVSC.2017.8366649).
- 76 D. Colombara, Anisotropy-induced fluctuations in Cu(In,Ga)Se<sub>2</sub>, *2022 IEEE 49th Photovoltaics Specialists Conference (PVSC)*, 2022, DOI: [10.1109/PVSC48317.2022.9938586](https://doi.org/10.1109/PVSC48317.2022.9938586).

